Available online at www.sciencedirect.com
ScienceDirect
Journal of Non-Crystalline Solids 354 (2008) 399–403
JOURNAL OF NON-CRYSTALLINE SOLIDS
www.elsevier.com/locate/jnoncrysol

Incipient amorphous-to-crystalline transition in HfO_2 as a function of thickness scaling and anneal temperature

Patrick S. Lysaght [a,*], Joseph C. Woicik [b], M. Alper Sahiner [c], Byoung-Hun Lee [a], Raj Jammy [d]

[a] *SEMATECH, 2706 Montopolis Drive, Austin, TX 78741-6499, United States*
[b] *National Institute of Standards and Technology, Gaithersburg, MD 20899, United States*
[c] *Seton Hall University, Physics Department, 400 S. Orange Avenue, South Orange, NJ 07079, United States*
[d] *IBM Assignee @ SEMATECH, 2706 Montopolis Drive, Austin, TX 78741-6499, United States*

Available online 26 October 2007

Abstract

A series of 1.4, 1.8, and 4.0 nm thick HfO_2 films deposited on Si(100) substrates have been measured by extended X-ray absorption fine-structure prior to anneal processing, following a standard post deposition anneal of 700 °C for 60 s in NH_3 ambient, and following an additional rapid thermal anneal cycle of 1000 °C for 10 s in N_2 ambient. Analysis of the second coordination shell gives clear evidence of increased ordering with increasing film thickness at each temperature. Similarly, increased ordering with increasing anneal temperature is evident for each film thickness. Although X-ray diffraction and high resolution transmission electron microscopy indicated the 1.4 nm HfO_2 samples to be amorphous, EXAFS has distinguished nanocrystalline from amorphous states for these films.
© 2007 Elsevier B.V. All rights reserved.

PACS: 61.82.Rx; 61.10.Ht

Keywords: Crystallization; Nanocrystals; Sychroton radiation; X-ray absorption; X-ray fluorescence

1. Introduction

An industry wide effort to incorporate a thin Hf-based high-k ($k \approx 12$–25) gate dielectric film to replace SiO_2 ($k = 3.9$) while maintaining the prescribed rate of device scaling [1], has given rise to electrical performance enhancements due to improvements in the chemical engineering of thin dielectric films [2]. Correspondingly, interface performance enhancements of high-k/Si(100) systems have been realized [3], along with recent efforts to increase the permittivity of high-k materials through controlled incorporation of lanthanide series elements [4,5]. Central to all advanced dielectric film optimization endeavors has been the desire to circumvent crystallization of HfO_2 by alloying with Si and N to minimize adverse effects associated with precipitated impurity concentrations that may exacerbate leakage current pathways associated with grain boundary formation [6]. Concurrently, high resolution spectroscopic techniques capable of characterizing subtle film and interface stoichiometric variations as a function of gate stack layer deposition and subsequent anneal processing have emerged as critical requirements for the identification of microstructure driven mechanisms that limit the electrical performance of Hf-based complimentary metal oxide semiconductor (CMOS) devices [7].

Extended X-ray absorption fine-structure (EXAFS) spectroscopy is well suited for probing local structural distortions in thin HfO_2 as a function of anneal processing since this technique is sensitive to correlations on a length scale of a few Angstroms. EXAFS provides details regarding X-rays absorption by an atom (Hf) at energies near and above the core-level binding energies of that

* Corresponding author.
E-mail address: pat.lysaght@sematech.org (P.S. Lysaght).

0022-3093/$ - see front matter © 2007 Elsevier B.V. All rights reserved.
doi:10.1016/j.jnoncrysol.2007.07.050

atom such that the absorption spectra are especially sensitive to the formal oxidation state, coordination chemistry, distances, coordination number, and species of the atoms immediately surrounding the selected absorbing element [8]. An incident X-ray is absorbed by a Hf atom when the energy of the X-ray is transferred to a core-level electron (L shell) which is ejected from the Hf atom. The atom is left in an excited state with an empty electronic level (a core-hole). Any excess energy from the incident X-ray is given to the ejected photoelectron. EXAFS captures interference effects and depends on the wave nature of the ejected photoelectron [9]. Ideally, if the scattering properties (scattering amplitude, phase shift, and mean free path) of the neighbor atom are known, one can determine the distance to the neighbor atom, the coordination number of the neighbor atom, and the mean-square disorder of the distance to the neighbor atom. Since both the scattering amplitude and phase shift depend on the atomic number, EXAFS is also sensitive to the Z of the neighbor atom [10].

2. Experimental

HfO_2 blanket thin films were produced by atomic layer deposition (ALD) via precursor material tetrakis(ethylmethylamino)hafnium with ozone oxidation, (TEMAHf) + O_3, on Si(100) surfaces prepared with chemical oxide. The substrate temperature was maintained at 330 °C, while a specified number of ALD cycles, corresponding to the desired HfO_2 thickness based on a growth rate of ~0.08 nm/cycle, was executed. Kirsch et al. [11] determined the scaling limit of HfO_2 to be 15 ALD cycles ($T_{phys} = 1.2 \pm 0.2$ nm) where electrical results concur with physical evidence (X-ray reflectivity (XRR) density determination, low energy ion scattering (LEIS) continuity – completeness of film coverage, and X-ray photoelectron spectroscopy (XPS) chemical state determination), suggesting that film thickness scaling down to 1.2 nm is the physical limit such that the material begins to deviate from bulk HfO_2 properties. Interestingly, transistor results exhibit an improvement trend in both peak and high field mobility as HfO_2 thickness scales from 3.3 to 1.2 nm. This is likely due to reduced charge trapping and reduced Coulomb scattering. These results have stimulated additional enthusiasm for high resolution physical characterization in order to elucidate any microstructure variations directly corresponding to the performance advantages associated with scaling the HfO_2 film thickness. To that end, an EXAFS study has been performed on a series of scaled thickness, uncapped HfO_2 blanket films ($T_{phys} = 1.4$, 1.8, and 4.0 nm), following each of the three fundamental thermal cycles standard to conventional device processing: (i) as-deposited at 330 °C, (ii) post deposition anneal (PDA) at 700 °C for 60 s in NH_3 ambient, and (iii) PDA plus rapid thermal anneal (RTA) at 1000 °C for 5 s in N_2 ambient.

The Hf L_3-edge EXAFS experiments were performed at the National Synchrotron Light Source (NSLS) at Brookhaven National Laboratory (BNL) on beamline X23A2, operated by the National Institute of Standards and Technology (NIST). EXAFS data were acquired in the fluorescence detection mode with a 5° angle of X-ray incidence. Since EXAFS is an interference effect which depends on the wave nature of the ejected photoelectron, it is practical to express the data in terms of photoelectron wave-number, k, which has the dimensions of 1/distance. As the incident X-ray energy E increases above the absorption threshold E_0 (Hf L_3-edge = 9561 eV), the kinetic energy of the photoelectron $E - E_0$ increases correspondingly. Likewise, its momentum $\hbar k$ and wavelength $2\pi/k$ (related by conservation of energy, $\hbar^2k^2/2m = E - E_0$, where m is the electron mass) also vary with E, as $k = [(E - E_0)/\hbar^2]^{1/2}$ [12]. The $\chi(k)$ functions were extracted by subtracting the atomic absorption background using the AUTOBK code [13]. These functions are then Fourier Transformed (FT) using a Gaussian window set for 2.0–12.5 Å k-range. Analysis of the FT data provides information on the near-neighbor coordination, distance, and the local disorder around the Hf absorbing atom obtained using the multiple scattering EXAFS calculation code FEFF 8.2 developed at the University of Washington [14].

Fig. 1 illustrates a set of FEFF 8.2 calculated theoretical EXAFS reference functions (standards) for monoclinic, orthorhombic, and tetragonal phases of HfO_2 crystal structures which identify the corresponding scattering paths contributing to the FT data. These calculated references have been rendered without Debye–Waller factors which would provide some reduction factor for the intensity of coherent (Bragg) scattering arising from thermal motion of the atoms in the lattice and with the assumption of pure phases with theoretical coordination numbers. Although the peak intensities are different from the experimental data, the peak locations and shapes offer valid phase identification comparisons with the measured FT data set for these samples.

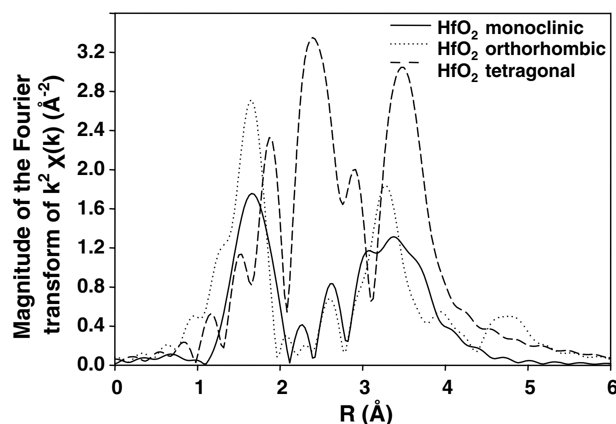

Fig. 1. The reference FEFF 8.2 calculated monoclinic, orthorhombic, and tetragonal phases of HfO_2.

3. Results and discussion

The physical and electrical performance quality of the interface between like crystal grains, where atomic planes are disrupted to some extent, may be defined by the relative rotational misorientation of the two grains, the orientation of the grain boundary plane between them, and any translations of the two adjacent crystallites relative to one another [15]. While this is difficult to accurately characterize for HfO_2 gate dielectric thin films where typical grain size is on the order of ~5–10 nm, the volume fraction of order may be diminished as film thickness decreases due to surface energy effects and the large surface area to volume ratio such that crystallization may ultimately be circumvented entirely. Typical of material that lowers its free energy by nucleation and growth of crystallites, HfO_2 crystallization of the tetragonal phase is associated with a larger decrease in free energy compared to the cubic phase [16]. The tetragonal phase can then transform to monoclinic. This explains why the cubic polymorph is never observed [17–19].

Fig. 2(a) illustrates the FT EXAFS data for 1.4, 1.8, and 4.0 nm thick HfO_2 prior to anneal processing ($T_{\text{deposition}} = 330\,°C$) and the influence of the PDA process on each of these films may be seen by comparison with Fig. 2(b). It is difficult to interpret the second order peaks conclusively for the unannealed samples since they all appear to be amorphous and definitive order around this radial distance R(Å) is not expected prior to any type of annealing. By contrast, the double peak feature just beyond 3 Å radial distance, for the calculated monoclinic structure in Fig. 1, clearly emerges in the 4.0 nm HfO_2 film following PDA (Fig. 2(b)). This degree of identifiable order is not exhibited by the two thinner films at the same temperature. The first shell peak around 1.9 Å corresponds to seven nearest neighbor O atoms in the monoclinic structure. The second shell peak around 3.0 Å is dominated by Hf–Hf backscattering [20]. In the first shell, Hf–O scattering amplitude and phases were used. In the second shell, multiple scattering from Hf–O–O paths were negligible compared with Hf–Hf contribution. The high temperature set of incremental thickness HfO_2 films is shown in Fig. 3(a) where they have been measured and transformed following the PDA (700 °C for 60 s in NH_3) + RTA (1000 °C for 10 s in N_2 ambient) process. The FT EXAFS data for Fig. 3(b) illustrates the relevant similarity of the measured 4.0 nm HfO_2 film annealed by PDA + RTA compared with a measured standard monoclinic HfO_2 powder sample. Second order peaks of the PDA (Fig. 2(b)) and PDA + RTA (Fig. 3(a)) samples are likely due to the coexistence of monoclinic and tetragonal phases with the monoclinic phase contributing a double peak structure beyond 3 Å,

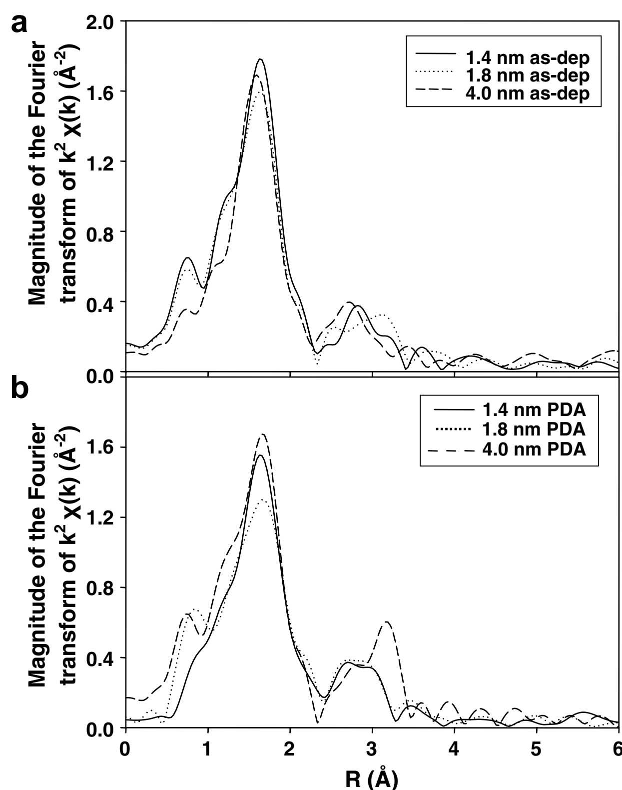

Fig. 2. The Fourier transformed EXAFS data for 1.4, 1.8, and 4.0 nm thick HfO_2 (a) prior to anneal processing (330 °C deposition temperature) and (b) following the PDA process of 700 °C for 60 s in NH_3 ambient.

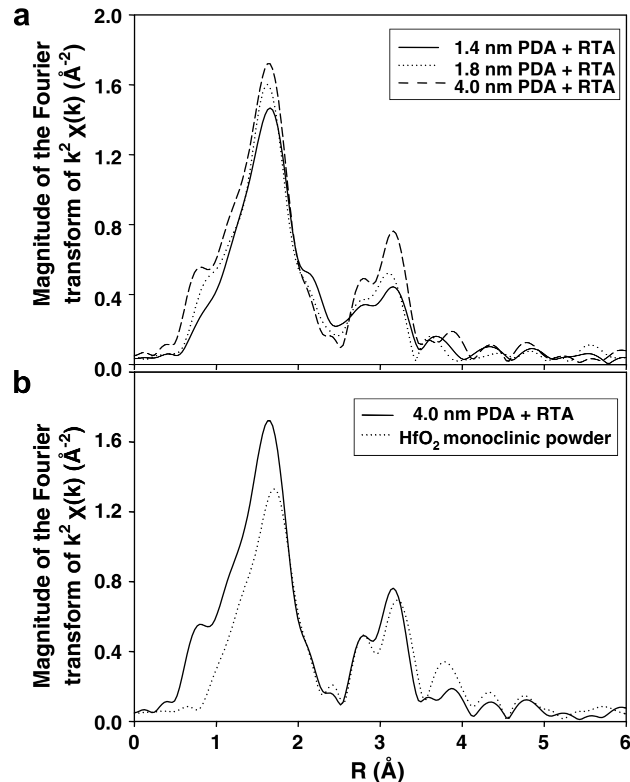

Fig. 3. The Fourier transformed EXAFS data for 1.4, 1.8, and 4.0 nm thick HfO_2 (a) following the PDA (700 °C for 60 s in NH_3) + RTA (1000 °C for 10 s in N_2 ambient) process and (b) the Fourier transformed EXAFS data for 4.0 nm HfO_2 following PDA + RTA shown with a measured monoclinic HfO_2 reference powder sample.

Table 1
Fourier transformed XAFS data and the non-linear least square fits for the second shell for the annealed samples

Sample ID	Second shell fits			
	Tetragonal ($P4_2/nmc$)		Monoclinic ($P2_1/c$)	
	$R_{Hf–Hf}$ (Å)	$N_{Hf–Hf}$	$R_{Hf–Hf}$ (Å)	$N_{Hf–Hf}$
1.4 nm PDA	3.38	10.3	3.19	3.2
1.8 nm PDA	3.57	9.7	3.38	4.1
4.0 nm PDA	3.70	8.4	3.51	5.4
1.4 nm PDA + RTA	3.68	7.4	3.49	5.8
1.8 nm PDA + RTA	3.65	7.8	3.47	6.1
4.0 nm PDA + RTA	3.62	6.9	3.37	6.5

with the strong tetragonal phase peak around 2.5 Å. This phenomenon may influence the second order peaks of the 1.4 and 1.8 nm PDA samples, which exhibit a single broad peak. Table 1 illustrates the FT EXAFS data and the non-linear least square fits for the second shell for each of the annealed samples. R(Å) values indicate average Hf–Hf distances in the second shell. The theoretical values for the Hf–Hf coordination numbers ($N_{Hf–Hf}$) in the second shell is 12 and 7 for the tetragonal (space group $P4_2/nmc$) and the monoclinic (space group $P2_1/c$) phases, respectively. The data in Table 1, therefore, indicates a transition from tetragonal to monoclinic phase with (i) increasing anneal temperature for each film thickness and with (ii) increasing film thickness at a specific anneal temperature. The uncertainties in R and $N_{Hf–Hf}$ values are ±0.03 Å and ±1.0, respectively. Attempts to fit the measured peaks of the PDA and PDA + RTA samples with combinations of the calculated orthorhombic (space group Pbca) and monoclinic phases were not successful.

4. Conclusion

The local structures of scaled HfO_2 thin films were probed by X-ray absorption spectroscopy. Consider the

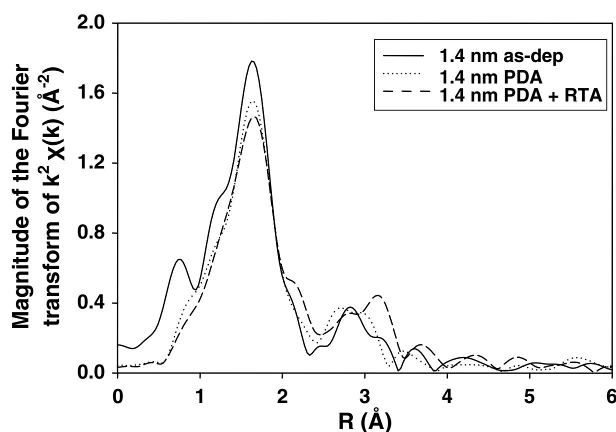

Fig. 4. The Fourier transformed EXAFS data for the 1.4 nm thick HfO_2 material for each of the three temperatures, as-deposited (330 °C), following the PDA process and following the PDA + RTA process.

1.4 nm HfO_2 sample measured at each of the three temperatures and illustrated in Fig. 4. Although X-ray diffraction (short range order limit of ∼3–4 nm) and high resolution transmission electron microscopy images taken in cross-section (as well as plan-view imaging), indicated the 1.4 nm HfO_2 film exposed to PDA + RTA anneal processing to be amorphous, such that no contrast evidence of order could be detected, the EXAFS data for this sample clearly indicate evidence of monoclinic structure.

EXAFS clearly show that an increase in the HfO_2 film thickness and anneal temperature increases the Hf–Hf coordination number, $N_{Hf–Hf}$, toward the monoclinic phase value of 7 which is consistent with a greater degree of crystallization. Furthermore, the monoclinic phase is suppressed for the 1.4 and 1.8 nm samples as-deposited and following the PDA process, but each of the three thicknesses of HfO_2 exhibit evidence of monoclinic phase composition following PDA + RTA annealing, whereby the scale of order trends with film thickness.

Acknowledgement

This work has been supported by Research Corporation Award #CC6405 and NSF DMI-0420952.

References

[1] International Technology Roadmap for Semiconductors, 2005 Ed., 2005.
[2] M.A. Quevedo-Lopez, S.A. Krishnan, P.D. Kirsch, G. Pant, B.E. Gnade, R.M. Wallace, Appl. Phys. Lett. 87 (2005) 262902.
[3] G. Bersuker, C.S. Park, J. Barnett, P. Lysaght, P. Kirsch, C.D. Young, R. Choi, B.H. Lee, B. Foran, K. van Benthem, S. Pennycook, P. Lenahan, R. Jason, J. Appl. Phys. (2006).
[4] D. Kumar, C.R. Gautam, O. Parkash, Appl. Phys. Lett. 89 (2006) 112908.
[5] L.F. Edge, D.G. Schlom, S. Rivillon, Y.J. Chabal, M.P. Agustin, S. Stemmer, T. Lee, M.J. Kim, H.S. Craft, J.P. Maria, M.E. Hawley, B. Holländer, J. Schubert, K. Eisenbeiser, Appl. Phys. Lett. 89 (2006) 062902.
[6] P.S. Lysaght, P.J. Chen, R. Bergmann, T. Messina, R.W. Murto, H.R. Huff, J. Non-Cryst. Solids 303 (2002) 54.
[7] P.S. Lysaght, J. Barnett, J.C. Woicik, B. Foran, G. Bersuker, B.H. Lee, ECS Trans. 1 (5) (2006) 13.
[8] Matthew Newville, Consortium for Advanced Radiation Sources, University of Chicago, 2004.
[9] Y. Iwasawa (Ed.), X-ray Absorption Fine Structure, World Scientific Publishing, 1996.
[10] G. Friedlander, J.W. Kennedy, Nuclear and Radiochemistry, John Wiley, NY, 1955.
[11] P.D. Kirsch, M.A. Quevedo-Lopez, H.-J. Li, Y. Senzaki, J.J. Peterson, S.C. Song, S.A. Krishnan, N. Moumen, J. Barnett, G. Bersuker, P.Y. Hung, B.H. Lee, T. Lafford, Q. Wang, D. Gay, J.G. Ekerdt, J. Appl. Phys. 99 (2006) 023508.
[12] D.C. Koningsberger, R. Prins (Eds.), X-ray Absorption, John Wiley, NY, 1989.
[13] M. Newville, P. Livins, Y. Yacoby, J.J. Rehr, E.A. Stern, Phys. Rev. B 47 (1993) 14126.
[14] A.L. Ankudinov, B. Ravel, J.J. Rehr, S.D. Conradson, Phys. Rev. B 58 (1998) 7565.
[15] Y.M. Chaing, D. Birnie III, W.D. Kingery, Physical Ceramics, Principles for Ceramic Science and Engineering, John Wiley, 1997.

[16] M.L. Balmer, F.F. Lange, C.G. Levi, J. Am. Ceram. Soc. 77 (1994) 2069.
[17] G. Rayner, R. Therrien, G. Lucovsky, Mater. Res. Soc. Symp. 611 (2000) C1.3.1–C1.3.9.
[18] D.A. Neumayer, E. Cartier, J. Appl. Phys. 90 (2001) 1801.
[19] D.H. Aguilar, L.C. Torres-Gonzalez, L.M. Torres-Martinez, T. Lopez, P. Quintana, J. Solid State Chem. 158 (2000) 349.
[20] M.A. Sahiner, J.C. Woicik, P. Gao, P. McKeown, M.C. Croft, M. Gartman, B. Benapfl, Thin Solid Films 515 (16) (2007) 6548.